

Comparison studies on electrodeposited CdSe, SnSe and $Cd_xSn_{1-x}Se$ thin films

V. Dhanasekaran · Jongwan Jung · Kee Keun Lee · T. Mahalingam

Received: 27 August 2014 / Revised: 10 September 2014 / Accepted: 11 September 2014 / Published online: 27 September 2014
© Springer-Verlag Berlin Heidelberg 2014

Abstract Electroplated cadmium stannous selenide ($Cd_xSn_{1-x}Se$) thin films were coated on indium-doped tin oxide (ITO) conducting glass substrates from aqueous bath solutions containing $CdCl_2$, $SnCl_2$, and Na_2SeO_3 . The x value was tuned by change in metal ion source concentration of the electrolytic bath solution. The various x values such as 1, 0.7, 0.45, and 0, of $Cd_xSn_{1-x}Se$ thin films were characterized by structural, morphological, compositional, and optical properties using X-ray diffraction, scanning electron microscopy, energy dispersive analysis by X-rays, and UV-vis-NIR spectrophotometer, respectively. X-ray diffraction (XRD) patterns revealed that the deposited films exhibit polycrystalline nature $Cd_xSn_{1-x}Se$ thin films. The microstructural parameters such as crystallite size, dislocation density, microstrain, and number of crystallites per unit area were calculated and presented. Morphological studies revealed that spherical-shaped grains were observed in cadmium-dominated films and nano-rod-shaped grains were observed in tin-dominated films. Optical properties of $CdSnSe$ films were determined from optical transmittance data in the spectral range 400 to 1,100 nm. The optical direct transition energy band gap was estimated using conventional method, and band gap energy was lying between 1.02 and 1.83 eV. The refractive index, extinction coefficient, and real and imaginary parts of dielectric constants were

calculated using optical transmission spectra of $Cd_xSn_{1-x}Se$ thin films.

Keywords Semiconductors · Chemical synthesis · X-ray diffraction · Microstructure · Optical properties

Introduction

The uses of thin film polycrystalline semiconductors have attracted much interest in an expanding variety of applications in various electronic and optoelectronic devices. The technological interests in polycrystalline-based devices are mainly caused by their low production cost. Cadmium selenide is an interesting material because of its efficient room temperature electro-luminescence and nano-electric device [1, 2] applications. CdSe has been investigated for its potential applications in solar cells [3], photoconductors [4], thin film transistors [5], light-emitting diodes [6], and gamma-ray detectors [7]. Tin selenide thin films have numerous applications as an efficient solar cell material [8], memory switching devices [9, 10], and holographic recording system [11]. CdSe and SnSe have been studied in the form of both thin films [12, 13] and single crystals [14, 15]. CdSe is a narrow band semiconductor, and its optical band gap is 1.74 eV [16], whereas the band gap of SnSe is 0.9 eV [17]. SnSe belongs to the group of layer-type orthorhombic IV–VI compounds characterized by a strong anisotropy of the chemical bonds and physical properties. In earlier, Datta et al. [18] have reported electrocrystallized Cd–Sn–Se thin films by varying Sn^{2+} concentration in the solution bath. They have discussed about the X-ray diffraction, atomic force microscopy, and scanning electron microscopy studies of Cd–Sn–Se thin films. Also, they have observed that optoelectronic properties were determined by spectroscopic analysis and electrochemical measurements. Among the various methods used to prepare thin films are vacuum evaporation,

V. Dhanasekaran (✉) · J. Jung
Graphene Research Institute, Sejong University, Seoul 143-747,
South Korea
e-mail: v.j.dhanasekaran@gmail.com

J. Jung
Faculty of Nanotechnology & Advanced Materials Engineering and
Graphene Research Institute, Sejong University, Seoul 143-747,
South Korea

K. K. Lee · T. Mahalingam
Department of Electrical and Computer Engineering, Ajou
University, Suwon 443-749, South Korea

chemical vapor deposition [19, 20], and electrodeposition [21, 22]. Electrochemical deposition is the cheapest known technique for preparation of thin films. It is a slow process, which facilitates a better orientation of the crystallites with an improved grain structure. Our group previously published in electrochemical, structural studies of CdSnSe thin films with different electrochemical bath solutions [23, 24]. In this paper, we have reported the comparison studies of structural, optical, morphological, and compositional properties of the electrodeposited CdSe, Cd_xSn_{1-x}Se, and SnSe thin films.

Experimental details

The electrodeposited Cd_xSn_{1-x}Se thin films were grown using potentiostatic mode. A standard three-electrode cell was used for the electrodeposition of CdSnSe. Indium-doped tin oxide (ITO) was used as a working electrode, graphite rod as a counter electrode, and a saturated calomel electrode (SCE) as the reference electrode. ITO-coated glass substrates were first cleaned in acetone and thoroughly rinsed with distilled water. The deposition of CdSnSe thin films was carried out from an aqueous electrolyte bath containing 0.01–0.02 M, 0.01–0.02 M, and 0.005 M concentrations of CdCl₂, SnCl₂, and SeO₂, respectively. Also, we have used 0.02 M EDTA as a supporting electrolyte. The solution pH was adjusted to 2.5 ± 0.1 by the addition of NaOH solution. Electrodeposition was carried out using an electrochemical system consisting of PAR (EG&G Princeton Applied Research, USA Model 362A) potentiostat/galvanostat unit. An X-ray diffractometer system (X'PERT PRO PANalytical, Netherlands) with CuK_α radiation (λ=0.1540 nm) was used to identify the crystal structure of the films. Surface morphology was carried out using a scanning electron microscopy (Philips Model XL 30, USA). Optical properties of the samples were analyzed using a UV-Vis-NIR double beam spectrophotometer (HR-2000, M/S ocean optics, USA).

Results and discussion

X-ray diffraction analysis is a powerful tool for crystal structure and crystal imperfections properties of thin films. X-ray diffraction patterns are obtained for Cd_xSn_{1-x}Se films deposited at various *x* values such as 1, 0.7, 0.45, and 0, as shown in Fig. 1. The observed *d*-spacing values are in good agreement with standard JCPDS values (88-2346 & 89-0249). Figure 1a represents the diffraction pattern of Cd_xSn_{1-x}Se thin film prepared at *x*=1. In this, pattern revealed that the predominant peak orientation is observed at 25.12° for (111) crystallographic plane. Other dualistic peaks are observed at angles 42.85° and 48.80° for corresponding crystallographic plane (220) and (311), respectively. No other impurity peaks are observed in

this diffraction pattern. Figure 1b shows the X-ray diffraction pattern of Cd_{0.7}Sn_{0.3}Se thin film. When the *x* value is decreased from 1 to 0.7, the diffraction pattern is entirely changed. Because of the inclusion of tin atoms in Cd and Se, diffraction angles are shifted and novel SnSe diffraction lines are emerged. SnSe-related diffraction lines are observed at 30.12° and 31.23° corresponding to (111) and (130), respectively. In addition to that, (220) and (311) peaks are disappeared by introduction of *x*=0.3 atomic ratio Sn element in Cd_xSn_{1-x}Se thin film. Figure 1c shows the X-ray diffraction pattern of Cd_{0.45}Sn_{0.55}Se thin film, and it is discovered mix of cubic (CdSe) and orthorhombic (SnSe) structures. The diffraction peaks of cubic CdSe structure 2θ value is observed at 25.50° for (111) lattice orientation. While the diffraction peaks of orthorhombic SnSe structure diffraction angles are observed at 30.40°, 31.21°, and 44.18°, corresponding lattice planes are (111), (130), and (022), respectively. There are more “Sn” ions combined with surplus “Se” ions than “Cd” ions; it may be due to the bond length and atomic radius. Even though “Sn” element is a noble metal, it can easily access to form compound with chalcogenides. When the *x* value decreases from 0.45 to 0, the predominant peak is observed at (111) plane. Also, some other new peaks are observed at 25.61°, 30.91°, 37.38°, 41.51°, and 44.25°, corresponding to crystallographic plane (021), (040), (131), (002), and (022), respectively. All the peaks are identified from Cd_xSn_{1-x}Se alloy formation; hence, no additional lines observed correspond to individual elements of Cd, Sn, and Se.

The crystallize size of the electrodeposited Cd_xSn_{1-x}Se thin film can be calculated using full width at half maximum (FWHM) data and Debye-Scherrer formula [25]:

$$D = \frac{0.9\lambda}{\beta \cos\theta_B} \quad (1)$$

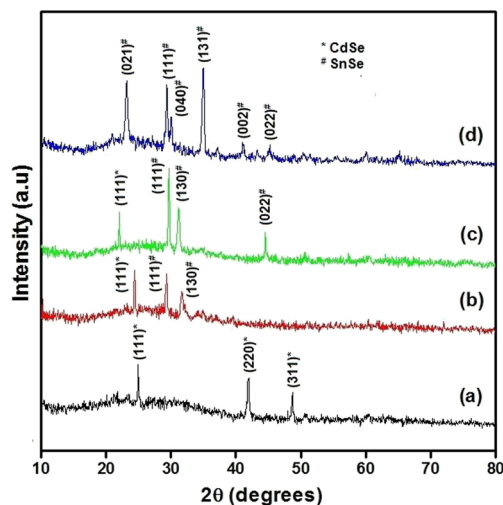


Fig. 1 X-ray diffraction pattern of Cd_xSn_{1-x}Se thin films at various composition ratio of Cd/Sn (a) 1:0 (b) 0.7:0.3 (c) 0.45:0.55, and (d) 0:1

where β is the full width at half maximum of the peak position in radiant, λ is the wavelength 1.540 Å, and θ_B is Bragg's diffraction angles. The calculated crystallite size is varied from 26.5 to 39.5 nm. It is observed from Fig. 2 that the x values decreased and crystallite sizes increased; it may be due to the improvement of crystallinity. In this, crystallinity improvement can be due to the more amount of “Sn” atoms incorporated in alloy films. Also, during the ternary compound formation in CdSe to CdSnSe thin film, the noble metal of Sn domination increases, which depends on the composition ratio. The “Sn” element decreases the crystallite size which may be due to the interaction between the atoms increased in ternary compounds. The crystallite size variation was studied in CdSe thin films by Sarangi and Sahu [26]. The dislocation density δ is defined as the length of dislocation lines per unit volume of the crystal and can be evaluated from the particle size D by the following relation:

$$\delta = \frac{n}{D^2} \tag{2}$$

where n is a factor, which equals unity giving minimum dislocation density. Figure 2 represents dislocation density variations of Cd_xSn_{1-x}Se thin film for different values of x . The dislocation density increases with decrease of x values; it may be attributed to decrease of crystallite size.

The microstrain ε value is calculated using the following relation [27]:

$$\frac{\beta \cos \theta}{\lambda} = \frac{1}{D} + \frac{\varepsilon \sin \theta}{\lambda} \tag{3}$$

The crystallite size is indirectly proportional to microstrain and dislocation density of the electrodeposited CdSnSe thin films. The x value decreases from 1 to 0.45; the microstrain, dislocation density, and number of crystallites per unit area of

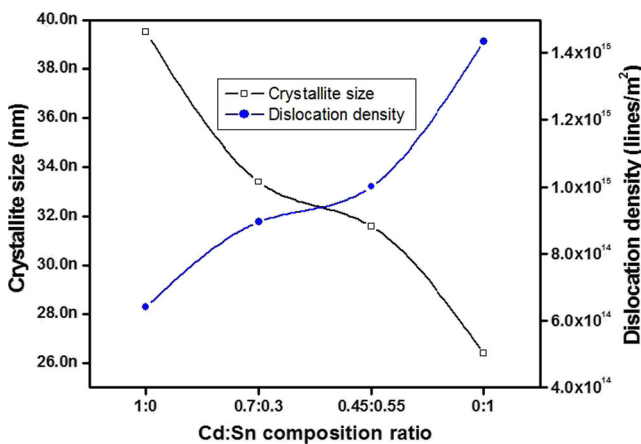


Fig. 2 Variation of crystallite size and dislocation density of Cd_xSn_{1-x}Se thin films

the Cd_xSn_{1-x}Se thin film values increase which are attributed to crystallite size decrease as shown in Fig. 3. The number of crystallites per unit area (N) of the films was determined using the following formula:

$$N = \frac{t}{D^3} \tag{4}$$

where t is thickness of the film, N is the number of crystallites per unit area, and D is the crystallite size. The number of crystallites per unit area is found to rapidly increase with decreases in x values. The number of crystallites per unit area increases which may be attributed to the reduction in crystallite size with increase in x values of Cd_xSn_{1-x}Se thin films shown in Fig. 3.

Optical transmission and reflection spectra are recorded at room temperature in air to obtain information on the optical properties of Cd_xSn_{1-x}Se thin films. The optical transmittance (T) and reflectance (R) spectrum of deposited Cd_xSn_{1-x}Se thin films in the wavelength range 300–1,200 nm. Optical transmission spectra of Cd_xSn_{1-x}Se thin film prepared at various values of x is shown in Fig. 4. The spectrum represented well-oriented grains build up the surface of the film. The high value of x has lowered the value of transmission, and decreased value of x increases the percentage of transmission. The observed transmission spectra is exhibited with semiinterferencefringes. In the absorption edges, the maxima and minima of the fringe of the reflectance spectrum, respectively, occur at the same wavelength positions of the minima and maxima of the transmittance spectrum, respectively. This is an indication of the optical homogeneity of the deposited films. The figure also shows a sharp fall of transmittance at the band edge, which is an indication of good crystallinity of the deposited films. The transmittance increases and it tends to increase in the UV to visible region. Besides, the optical transmittance decreases towards the IR region in electrodeposited Cd_xSn_{1-x}Se thin films. The increase in the transmittance is due to an increase

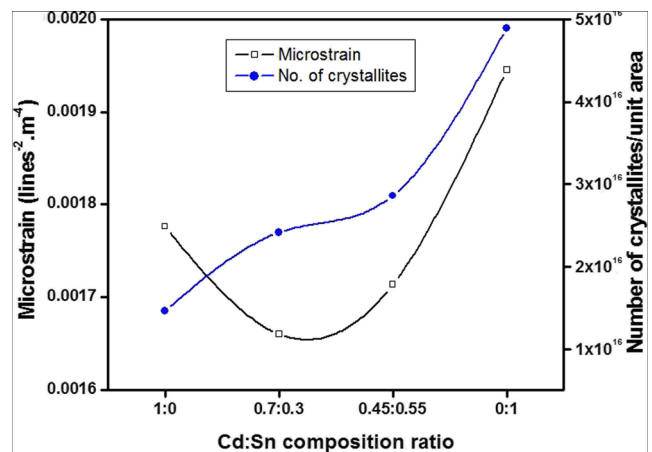


Fig. 3 Variation of microstrain and number of crystallites per unit area of Cd_xSn_{1-x}Se thin films

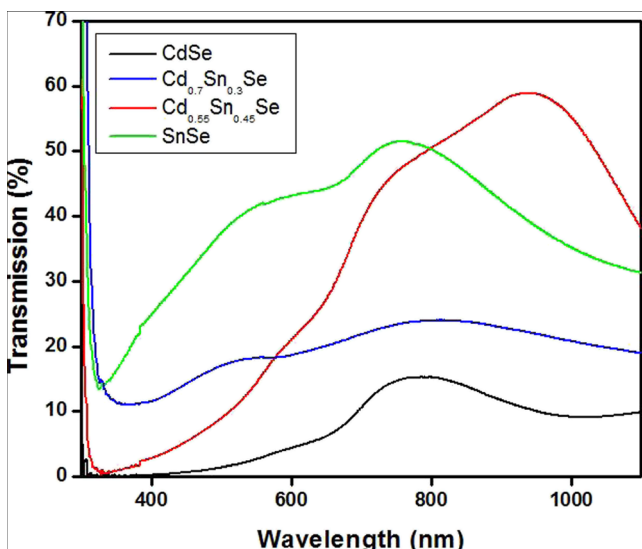


Fig. 4 Optical transmission spectra of Cd_xSn_{1-x}Se thin films

in the band gap with carrier concentration. The optical parameters such as absorption coefficient and band gap are determined from optical absorption measurements. The value of absorption coefficient for strong absorption region of thin film is calculated using Eq. (5) [28]:

$$\alpha = \frac{1}{t} \ln \left(\frac{A}{T} \right) \tag{5}$$

where α is the absorption coefficient (cm⁻¹), t is the thickness of the films, A is absorbance, and T is transmittance. The nature of transition is determined using the following equation [29]:

$$\alpha h\nu = A(h\nu - E_g)^n \tag{6}$$

where α is the absorption coefficient (cm⁻¹), $h\nu$ is a photon energy, E_g is an energy gap, A is an energy-dependent

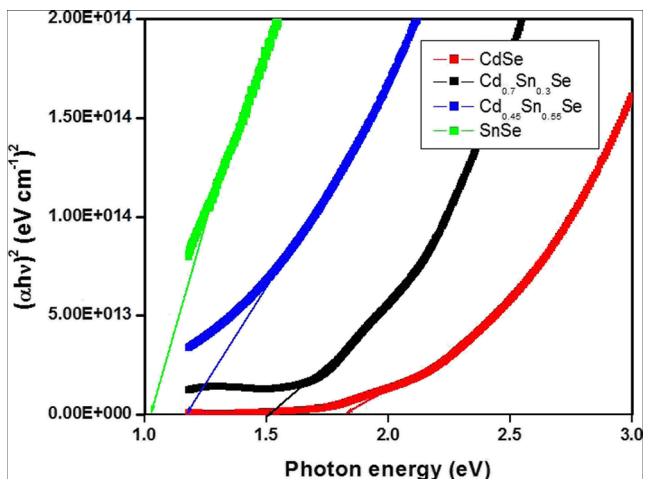


Fig. 5 Tauc's plot of Cd_xSn_{1-x}Se thin films

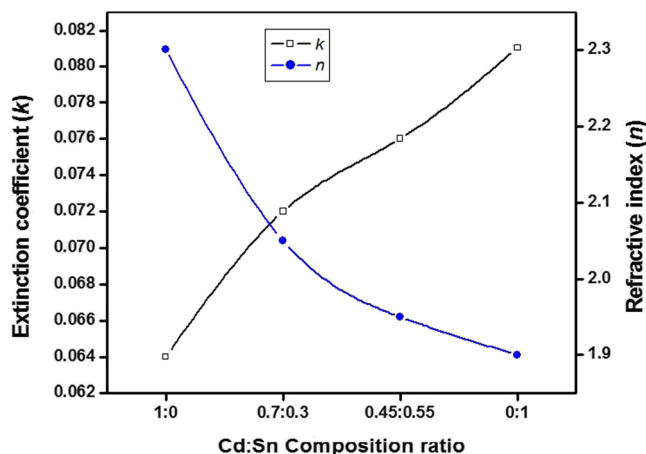


Fig. 6 Extinction coefficient and refractive index of Cd_xSn_{1-x}Se thin films

constant, and n is an integer depending on the nature of electronic transitions. For the direct allowed transitions, n has a value of 1/2 while for the indirect allowed transitions, $n=2$. The Tauc's plot of Cd_xSn_{1-x}Se thin film is shown in Fig. 5. The band gap energy is estimated to be 1.02 to 1.83 eV using conventional method. The CdSe band gap value is 1.83 eV, and band gap energy decreases with introduced “Sn” element in CdSe. This alloy formation of Cd_xSn_{1-x}Se thin film is a very good novel application in optoelectronic features.

The refractive index (n) and extinction coefficient (k) of Cd_xSn_{1-x}Se films are estimated using the following expressions [30]:

$$n = \frac{1 + R}{1 - R} + \sqrt{\frac{4R}{(1 - R)^2} - k^2} \tag{7}$$

$$k = \frac{\alpha \lambda}{4\pi} \tag{8}$$

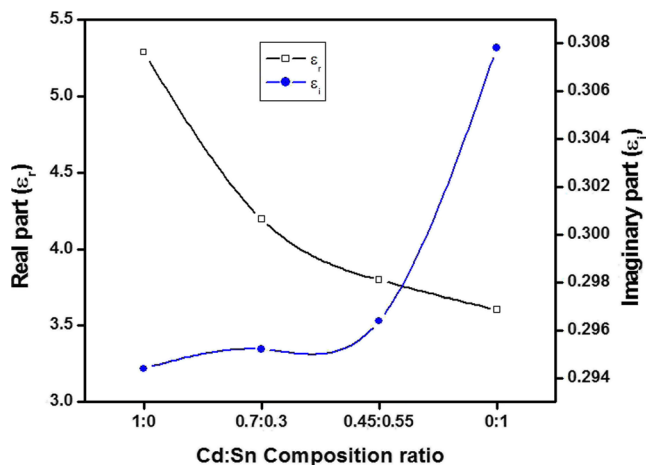


Fig. 7 Real and imaginary parts of dielectric constants of Cd_xSn_{1-x}Se thin films

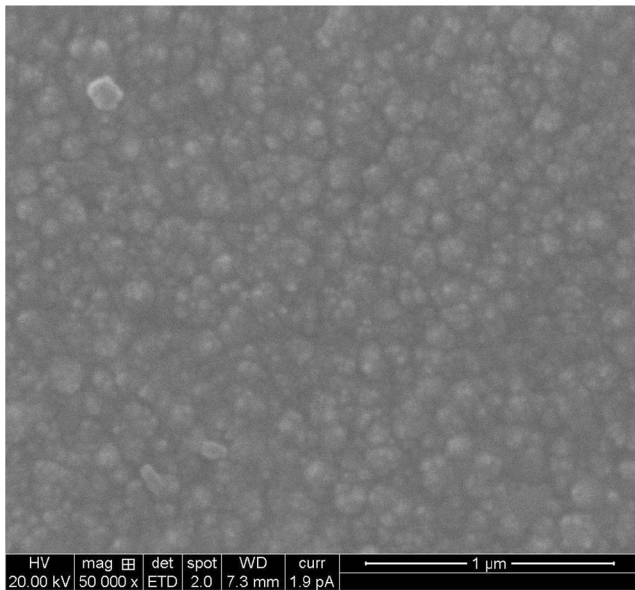


Fig. 8 Typical SEM picture of electrodeposited Cd₁Sn₀Se thin film

where α is the absorption coefficient, λ is the wavelength, and R is the reflectance of the Cd_xSn_{1-x}Se thin films. The refractive index and the extinction coefficient spectra of Cd_xSn_{1-x}Se thin films as a function of Cd/Sn composition ratio are shown in Fig. 6. It is observed from Fig. 6 that the refractive index decreases with x value decreases, while the extinction coefficient increases for electrodeposited Cd_xSn_{1-x}Se thin films. The value for the refractive index lies between 1.9 and 2.3, and the value of extinction coefficient lies between 0.064 and 0.08. It is attributed to the film thickness variation of Cd_xSn_{1-x}Se thin films.

The real and imaginary parts of the dielectric constant were determined using the following relation [30]:

$$\epsilon = \epsilon_r + \epsilon_i = (n + ik)^2 \tag{9}$$

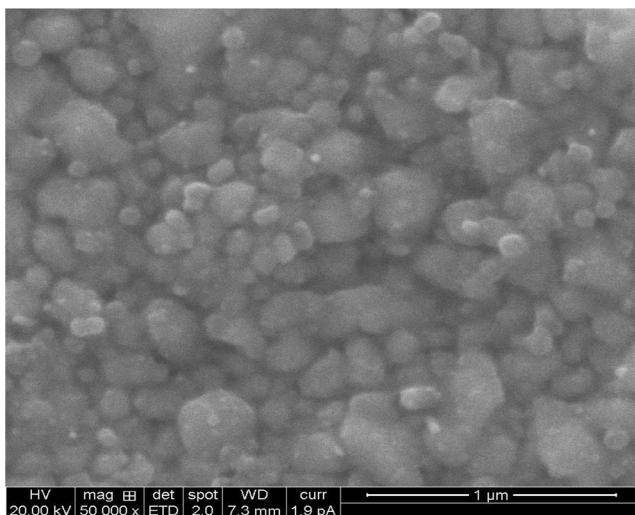


Fig. 9 Typical SEM picture of electrodeposited Cd_{0.7}Sn_{0.3}Se thin film

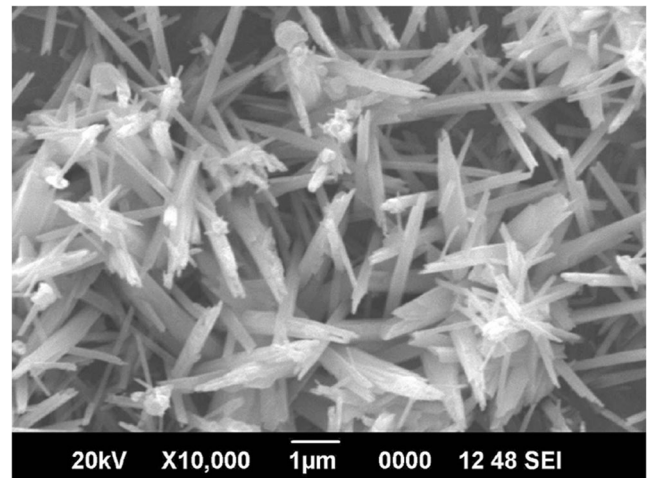


Fig. 10 Typical SEM picture of electrodeposited Cd_{0.45}Sn_{0.55}Se thin film

where ϵ_r and ϵ_i are the real and imaginary parts of the dielectric constant, respectively, and are given by the following relations:

$$\epsilon_r = n^2 - k^2 \tag{10}$$

and

$$\epsilon_i = 2nk \tag{11}$$

The imaginary part of the dielectric constant also showed the same behaviour as that of the real part; the only thing is that its values seem to be very less compared to real dielectric constant values. The real part of dielectric constant decreases, and imaginary part increases with decreases in x values as shown in Fig. 7.

The surface morphology of CdSe thin films has been analyzed using scanning electron microscopy. The films have a smooth surface with spherical grains (Fig. 8). The grains are distributed uniformly over the entire surface of the film with a

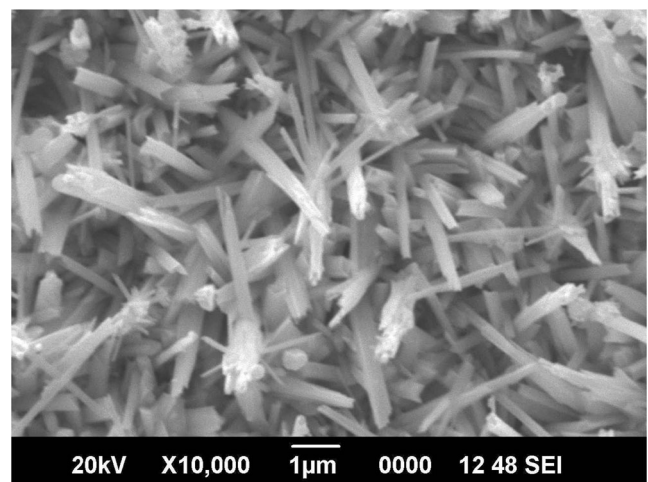


Fig. 11 Typical SEM picture of electrodeposited Cd₀Sn₁Se thin film

compact and fine grained morphology. At $x=1$, there is no complex surface formation occurred. The nucleation over growth and the film surface is covered with uniform spherical-shaped grain as shown in figure. The sizes of the grains are found to be in the range between 100 and 150 nm. Scanning electron micrograph of $\text{Cd}_{0.7}\text{Sn}_{0.3}\text{Se}$ thin film is shown in Fig. 9. The grains are small with non-uniform morphology, and no well-defined grain boundaries are observed; hence, it is difficult to calculate the average value of grain size. The reason for this state may be attributed to the tense state of the surface of the films. The grain sizes of CdSnSe thin film covered the entire surface of the film and are estimated to be in the range between the range of 150 and 200 nm. When the x value is decreased from 0.7 to 0.45, more grain growths occur; thereby, the average grain size is increased due to agglomeration of smaller grains together as shown in Fig. 10. It is also observed that nano-rod-shaped grains occupied the entire surface of the film. The grains tend to agglomerate, and the tension may be comparatively less in the films with the number of needle-like grains becoming less. It is evident that by altering the Cd and Sn element concentrations in the solution bath enhance the surface features. This nano-rod-like structure is a more featured observation in this alloy formation. This in turn allows the films to lower its total energy by grain growth and decrease in the grain boundary areas. The nano-rod-shaped grains are covered with small nano-needles protruding from the end of the nano-rods as shown in Fig. 11. Optical properties strongly depend on surface morphology of $\text{Cd}_x\text{Sn}_{1-x}\text{Se}$ thin films. The transmittance increase after introducing “Sn” element might be due to an increase of optical scattering caused by the densification of grains followed by grain growth and reduction of grain boundary density as depicted in Fig. 4.

Conclusions

Thin films of $\text{Cd}_x\text{Sn}_{1-x}\text{Se}$ with the combinations of $x=1, 0.7, 0.45$, and 0 were grown by electrodeposition technique. The crystalline sizes were controlled by varying the x values in the solution bath. X-ray diffraction patterns were taken out in order to determine crystal structure of the deposited film. The microstructural properties of $\text{Cd}_x\text{Sn}_{1-x}\text{Se}$ thin films were plausibly explained with the suitable compound formations. The optical transmission and reflection spectrum of the electrodeposited $\text{Cd}_x\text{Sn}_{1-x}\text{Se}$ thin films were recorded, and, using these results, direct transition energy band gap value was estimated in the range of 1.02–1.83 eV. SEM images revealed that the smooth and uniform surface was observed in $\text{Cd}_x\text{Sn}_{1-x}\text{Se}$ thin film, and nano-wires protruding from nano-rods of the surface morphology are observed at $x=0$. The $\text{Cd}_x\text{Sn}_{1-x}\text{Se}$ nano-structured grains with high surface-to-volume ratio as

optoelectronic materials are predicted, and this may be one of the materials for the construction of high efficiency optoelectronic devices.

Acknowledgments This research work was supported by the Basic Science Research Program through the National Research Foundation of Korea (NRF), funded by the Ministry of Education (2010-0020207, 2012R1A1A2007211).

References

1. Kelin DL, Roth R, Lim AKL, Alivisatos AP, McEuen PL (1997) *Nature* 389:699
2. Mattoussi H, Radzilowski LH, Dabbousi BO, Thomas EL, Bawendi MG, Rubner MF (1998) *J Appl Phys* 83:7965
3. Boudrau RA, Rauh RD (1982) *Sol Energy Mater* 7:385
4. Kainthla RC, Pandya DK, Chopra KL (1980) *J Electrochem Soc* 127: 277
5. Van Calster A, Vervaeet A, De Rycke I, De Baets J, Vanfleteren J (1988) *J Cryst Growth* 86:924
6. Ren J, Bowers KA, Sneed B, Dreifus DL, Cook JW Jr, Schetzina JF, Kolbus RM (1990) *Appl Phys Lett* 57:1901
7. Roth M (1989) *Nucl Instr Methods A* 283:291
8. Bletskan DI, Kopinets IF, Pogorsh PP, Salkora EN, Chepor DV (1978) *Kristallografiya* 20:1008
9. Rao TS, Ray BKS, Chaudhuri AK (1988) *Thin Solid Films* 165:257
10. Baxter CR, McLennan WD (1975) *J Vac Sci Technol* 12:110
11. Rodot M (1975) *Acta Electron* 18:345
12. Eriksson S, Gruszecki T, Carlsson P, Holmström B (1995) *Thin Solid Films* 269:14
13. Terada T (1971) *J Phys D* 4:1991
14. Burger A, Roth M (1984) *J Cryst Growth* 67:507
15. Agnihotri OP, Jain AK, Gupta BK (1979) *J Cryst Growth* 46:491
16. Lide DR, Frederikse HPR (eds) (1994) *CRC handbook of chemistry and physics*. CRC Press, Boca Raton, pp 12–95
17. Bhatt VP, Giresan K, Desai CF (1989) *Cryst Res Technol* 24:187
18. Dattaa J, Bhattacharya C, Bandyopadhyay S (2006) *Appl Surf Sci* 252:7493
19. John J, Pradeep B, Mathai E (1994) *J Mater Sci* 29:1581
20. Bennouna A, Tessier P, Priol M, Dang Tran Q, Robin S (1983) *Phys Status Solidi* 117:51
21. Subramanian B, Mahalingam T, Sanjeeviraja C, Jayachandran M, Chockalingam MJ (1999) *Thin Solid Films* 357:119
22. Engelken RD, Berry AK, Van Doren TP, Boone JL, Shahnazary A (1986) *J Electrochem Soc* 133:581
23. Dhanasekaran V, Mahalingam T, Chandramohan R, Chu JP, Rhee J-K (2012) *J Mater Sci Mater Electron* 23:645–651
24. Mahalingam T, Dhanasekaran V, Chu JP, Kim T, Kim YD (2011) *ECS Trans* 35:61–68
25. Wang Y, Suna A, McHugh J, Hilinski EF, Lucas P, Johnson RD (1990) *J Chem Phys* 92:6927
26. Sarangi SN, Sahu SN (2004) *Phys E* 23:159
27. Clark AH (1980) In: Kazmerski LL (ed) *Polycrystalline and amorphous thin films and devices*. Academic, New York
28. Dhanasekaran V, Mahalingam T (2013) *Mater Res Bull* 48:3585–3593
29. Benramdane N, Murad WA, Misho RH, Ziane M, Kebbab Z (1997) *Mater Chem Phys* 48:119
30. Osuwa JC, Oriaku CI, Kalu IA (2009) *Chalcogenide Lett* 9:433–436